Modelling Simul. Mater. Sci. Eng. **19** (2011) 000000 (14pp) UNCORRECTED PROOF

Dislocation–vacancy interactions in tungsten

Z M Chen[1], M Mrovec[1,2] and P Gumbsch[1,2]

[1] Institut für Angewandte Materialien (IAM), Karlsruher Institut für Technologie (KIT), 76131 Karlsruhe, Germany
[2] Fraunhofer-Institut für Werkstoffmechanik IWM, 79108 Freiburg, Germany

Received 16 February 2011, in final form 8 June 2011
Published
Online at stacks.iop.org/MSMSE/19

Abstract

We systematically investigate the interaction between a monovacancy and various lattice dislocations in body-centered cubic (bcc) metal tungsten by means of atomistic simulations. Two models with a different level of sophistication have been employed for the description of interatomic interactions—the empirical Finnis–Sinclair potential, which is a central-force scheme, and the bond-order potential, which is able to describe correctly unsaturated directional covalent bonds that are crucial for the cohesion and structure of bcc transition metals. Our simulation results show that the vacancy–dislocation interaction depends sensitively on the separation distance and orientation of the two defects. A comparison of the simulation results with the predictions of elasticity theory shows excellent agreement between the two approaches when the separation between the vacancy and the dislocation core is above 0.5 nm. Large deviations from the elastic limit are found at close distances, when the vacancy enters the dislocation core.

(Some figures in this article are in colour only in the electronic version) AQ1

1. Introduction

Many important metallurgical phenomena such as high-temperature creep, dislocation or 'pipe' diffusion, irradiation embrittlement and fracture are affected by the interactions between dislocations and point defects. Creep is associated with a non-conservative climb of dislocations by emission or absorption of vacancies. Pipe diffusion along dislocations may accelerate the diffusion of impurities by several orders of magnitude [1] or promote nucleation and growth of voids [2]. A supersaturation of vacancies in irradiated or heavily deformed materials significantly alters the mobility of dislocation both at high and low temperatures [3, 4], and can have a profound influence on fracture processes [5, 6].

A thorough understanding of all these phenomena rests ultimately on the knowledge of the underlying atomic processes that occur within a few nanometers from the interacting defects. Unfortunately, experimental observations of such complicated nano-scale phenomena are difficult to perform even with modern techniques. For this reason, most analyses of the

0965-0393/11/000000+14$33.00

JNL: MSMS PIPS: 385440 TYPE: SPE TS: NEWGEN DATE: 8/7/2011 EDITOR: TT SPELLING: US

point defect–dislocation interactions have been done using elasticity theory [7–9]. However, approximations have to be made for processes that are controlled by atomic mechanisms. In particular, when the core of the dislocation is involved in the interaction process, the continuum elasticity ceases to be applicable and a correct description of the interaction can only be obtained using an atomistic model [10].

The amount of research on dislocation–vacancy interactions by means of atomistic simulations carried out so far has been rather limited, especially for body-centered cubic (bcc) metals. Several studies of vacancies interacting with edge dislocations in α-iron [11] and molybdenum [12] were performed more than 30 years ago using simple pair potentials . A calculation based on an approximate tight-binding scheme was also done for the $1/2\langle 1\,1\,1\rangle$ screw and edge dislocations [13]. Most of these studies, however, concentrated on the variability of interaction outcomes using different interatomic potentials and paid little attention to the comparison between atomistic results and elasticity theory. Only recently, Clouet [14] carried out a thorough analysis of atomistic and elastic contributions for the interaction between vacancies and edge dislocations in several face-centered cubic metals, and showed that the atomistic and linear elastic predictions agree when the cores of the two defects do not overlap. Another very recent atomistic study of vacancy migration around a mixed edge-like dislocation in bcc iron was presented by Lau *et al* [15]. The results of this study were used in a kinetic Monte Carlo simulation of dislocation climb over extensive time and length scales [16].

A critical aspect of all atomistic simulations is their dependence on the description of interatomic interactions. Methods based on the density functional theory (DFT) provide such description most reliably and have been employed in many investigations of the physical and mechanical properties of materials (for reviews, see e.g. [17–19]). However, these calculations are limited to small block sizes and further restricted by the use of periodic boundary conditions. Consequently, studies of large and complex systems typically require approximations and significant simplifications when describing interatomic interactions. In large-scale atomistic studies of metallic materials the Finnis–Sinclair (FS) potential [20] has been one of the most broadly used methods describing the interatomic forces [21–23]. This central-force many-body potential is able to describe well simple and noble metals, in which the bonding is almost nearly free-electron-like. However, in transition metals such as tungsten, the bonding mediated by the d-electrons has a covalent and non-central character, which makes the bonds dependent also on the angles [24, 25]. The bond-order potential (BOP) is a method based on the tight-binding approximation and therefore it is able to describe correctly the angular character of bonding [26–28]. Despite its quantum mechanical origin, BOP is sufficiently computationally efficient for the modeling of extended defects and due to its real space formalism it is not limited by the periodic boundary conditions. In our study, we employ both BOP and the FS potential not only to investigate how sensitive is the outcome of the vacancy–dislocation interactions on the description of interatomic interactions but also to see whether it is possible to identify general results, which are independent of the model used.

The purpose of this paper is to describe the results of a systematic atomistic computer simulation study of the interactions between a monovacancy and four different dislocations in bcc tungsten. The dislocations investigated are $1/2\langle 1\,1\,1\rangle$ and $\langle 1\,0\,0\rangle$ screw dislocations, and $1/2\langle 1\,1\,1\rangle\{1\,1\,0\}$ and $\langle 1\,0\,0\rangle\{1\,1\,0\}$ edge dislocations. The reason for choosing the $1/2\langle 1\,1\,1\rangle$ screw dislocation is rather obvious. It has been firmly established by many experimental and theoretical studies [9, 29–31] that the specific plastic behavior of bcc metals at low temperatures can be attributed to a non-planar core configuration of the $1/2\langle 1\,1\,1\rangle$ screw dislocation. As a consequence, the $1/2\langle 1\,1\,1\rangle$ screw has a high Peierls stress and moves by a thermally activated formation of double kinks. It is still an open question how the interaction with a vacancy can influence this process. In contrast, the $1/2\langle 1\,1\,1\rangle$ edge (and mixed) dislocations possess an

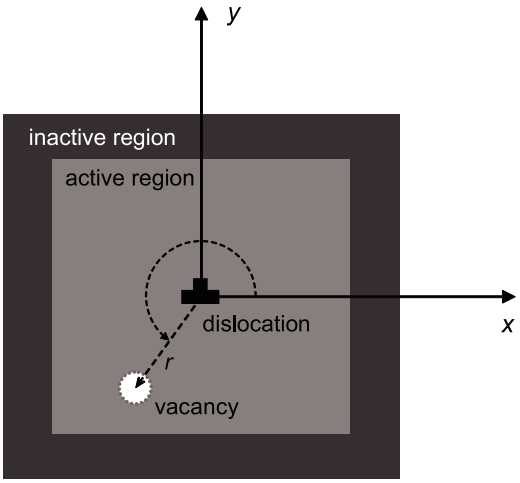

Figure 1. Schematic picture of the block used in the simulations. The dislocation is introduced at the center of the block by displacing all atoms according to the anisotropic elastic displacement field; the dislocation line lies parallel to the z direction. Atoms in the inactive region are kept fixed during the simulations. The dislocation–vacancy separation distance and relative angle are labeled r and θ, respectively.

extremely low lattice friction, and even a small attractive force, e.g. from a vacancy, may cause the dislocation to move in its slip plane [11]. Dislocations with the $\langle 1\,0\,0\rangle$ Burgers vector can be produced by interactions between the $1/2\langle 1\,1\,1\rangle$ dislocations [32–34]. They have usually been found as parts of dislocation networks. However, long and wavy $\langle 1\,0\,0\rangle$ dislocations have also been found in certain single crystals deformed to stage I [35]. Although it is generally assumed that dislocations with the $\langle 1\,0\,0\rangle$ Burgers vectors do not contribute directly to the plastic deformation, they are believed to play an important role in crack nucleation [36–39].

2. Method

2.1. Interatomic potentials

The atomistic simulations in this work were performed using two interatomic potentials developed for W—the FS potential [20, 40] and the BOP [27]. The FS potentials have been widely used to study lattice defects in metals as they are computationally efficient, but since they are central-force schemes their ability to describe the unsaturated directional covalent bonds of middle transition metals is limited. The BOPs are based on the tight-binding approximation and thus provide a direct bridge between electronic structure and atomistic approaches. Atomistic studies employing these potentials are therefore more likely to reveal correctly the structures and properties of lattice defects that induce changes in both bond lengths and bond angles.

2.2. Simulation block

The simulation block used in our calculations is depicted schematically in figure 1 and its main characteristics are given in table 1. The rectangular block is periodic along the z direction, which is also the direction of the dislocation line. Therefore, the initial dislocation in our simulations is always straight and infinite without any kinks or jogs. The periodic length of the block in the z direction in all simulations is at least 0.9 nm in order to minimize interactions

Table 1. Dimensions of simulation blocks (lattice parameter $a = 0.316\,52$ nm).

Dislocation type	X	Y	Z	Number of atoms
$1/2\langle 1\,1\,1\rangle$ screw	$40a$	$40a$	$4\sqrt{3}a$	∼11 000
$1/2\langle 1\,1\,1\rangle\{1\,1\,0\}$ edge	$60a$	$40a$	$2\sqrt{6}a$	∼24 000
$\langle 1\,0\,0\rangle$ screw	$40a$	$40a$	$3a$	∼10 000
$\langle 1\,0\,0\rangle\{1\,1\,0\}$ edge	$60a$	$40a$	$2\sqrt{2}a$	∼12 000

between periodic images of vacancies (see below). In the x and $y$directions perpendicular to the dislocation line rigid boundary conditions are used. In this setup, the atoms in the outmost 'inactive' region (see figure 1) are kept fixed so that the dislocation is effectively placed in an infinite crystal environment. The dimensions of the block in the x and $y$directions are about 12 nm for the screw dislocation simulations, whereas for the edge dislocation simulations the size along the x directions is multiplied by a factor of 1.5 since the edge cores are extended more along their glide planes [41]. The dislocations are introduced at the center of the perfect block by displacing the atoms according to the anisotropic elastic displacement field of a screw or an edge dislocation in an infinite medium [42]. In order to obtain realistic core structures, the atomic positions are then fully relaxed using a Fast Inertial Relaxation Engine (FIRE) [43]. The relaxation is considered complete when the forces on all atoms fall below 0.01 eV Å^{-1}. The vacancy is then introduced by removing an atom at different sites around the dislocation and the energy is minimized for the second time.

As already noted above, due to the periodic boundary condition along the dislocation line, the introduced vacancy also repeats infinitely in the z direction with a separation distance of z_0 (1–2 nm, see table 1). Our tests, however, show that the vacancy–vacancy interactions for these separations are already very small and can be neglected. For instance, the binding energy for the $1/2\langle 1\,1\,1\rangle$ screw dislocation changes by less than 0.01 eV when the z dimension of the block and therefore also the vacancy repeat length are doubled. Thus, the simulation blocks used in our simulations are sufficiently large to capture the essence of the dislocation–vacancy interactions in a reliable manner.

3. Results

3.1. Core structures

The relaxed core structures are shown in figure 2, where the atomic arrangements are shown in the planes perpendicular to the dislocation lines. Atoms in different atomic layers are distinguished by different colors. The $1/2\langle 1\,1\,1\rangle$ screw dislocation is considered the most important dislocation in bcc metals since it controls the low-temperature plastic deformation. Crystallographically, the $\langle 1\,1\,1\rangle$ direction is a three-fold screw axis in the bcc lattice and hence the core structure of the screw dislocation parallel to this direction must also possess such a symmetry and be intrinsically non-planar [9, 31]. While direct experimental observations of the cores of screw dislocations are difficult [44, 45], the non-planar character of the core has been found in all atomistic calculations [10, 17, 27–29, 31, 46, 47] using a broad variety of descriptions of interatomic interactions.

In figure 2(a), the $1/2\langle 1\,1\,1\rangle$ screw dislocations are plotted using a differential displacement map [48]. The lengths of the arrows correspond to the displacements of two neighboring atoms parallel to the Burgers vector. Two types of cores are obtained: the FS potential yields a core that is rather extended and spread asymmetrically into three $\{1\,1\,0\}$ planes, and is not invariant with respect to the $[1\bar{1}0]$ diad symmetry operation (see figure 2(a1));

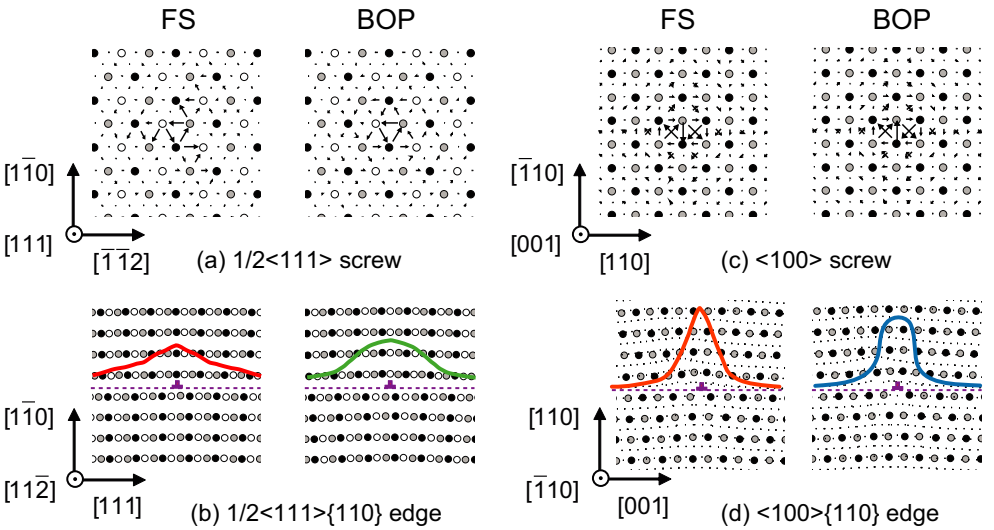

Figure 2. Relaxed dislocation core structures calculated using BOP and FS potentials. Circles with different shadings correspond to atoms in adjacent layers. The differential displacement method is used for plotting the cores of screw dislocations. For the edge dislocations, the densities of the Burgers vectors along the glide plane are illustrated.

the BOP gives a more compact core that is invariant with respect to this symmetry operation and spreads symmetrically (see figure 2(*a*2)). The two core variants are often termed as 'degenerate' and 'non-degenerate', respectively [49].

Unlike the screw, the core of $1/2\langle 1\,1\,1\rangle\{1\,1\,0\}$ edge dislocation shown in figure 2(*b*) is planar. A detailed analysis of the relaxed configurations reveals that the large inelastic displacements parallel to the Burgers vector are predominantly confined to a single $\{1\,1\,0\}$ atomic plane immediately above the slip plane and the Burgers vector is distributed widely along the glide plane [50]. As a consequence, the Peierls barrier is extremely low and the mobility of the edge dislocation is several orders of magnitude higher than the mobility of the screw.

As mentioned above, the $\langle 1\,0\,0\rangle$ dislocations have been found in experiments as products of reactions between the $1/2\langle 1\,1\,1\rangle$ dislocations. They can be of either screw or edge character. With both BOP and FS potentials the $\langle 1\,0\,0\rangle$ screw dislocations have similar non-planar cores whose centers are located between two atomic columns (see figure 2(*c*)). The $\langle 1\,0\,0\rangle\{1\,1\,0\}$ edge dislocations have planar core structures (see figure 2(*d*)), which are however much narrower than the cores of the $1/2\langle 1\,1\,1\rangle$ edge dislocations.

3.2. Dislocation–vacancy binding energy

Thermodynamically, the interaction between a dislocation and a vacancy is characterized by the interaction or binding energy, E_{bind}, which indicates whether it is more favorable for the vacancy to remain in the bulk or in the vicinity of the dislocation. This energy can be determined easily from total energies of four different atomic configurations as

$$E_{\text{bind}} = (E_{\text{vac,dislo}} - E_{\text{dislo}}) - (E_{\text{vac}} - E_{\text{ideal}}), \tag{1}$$

where E_{ideal} is the total energy of the ideal block without any defect and E_{dislo}, E_{vac} and $E_{\text{vac,dislo}}$ are the total energies of relaxed blocks containing a single dislocation, a single vacancy, and

Table 2. Vacancy formation energies (eV).

FS	BOP	DFT[a,b]	Exp.[a,b]
3.6	3.8	3.3–3.8	3.5–4.1

[a] Foiles S M 1993 Interatomic interactions for Mo and W based on the low-order moments of the density of states *Phys. Rev.* B **48** 4287.
[b] Soerlind P, Yang L H, Moriarty J A and Wills J M 2000 First-principles formation energies of monovacancies in bcc transition metals *Phys. Rev.* B **61** 2579.

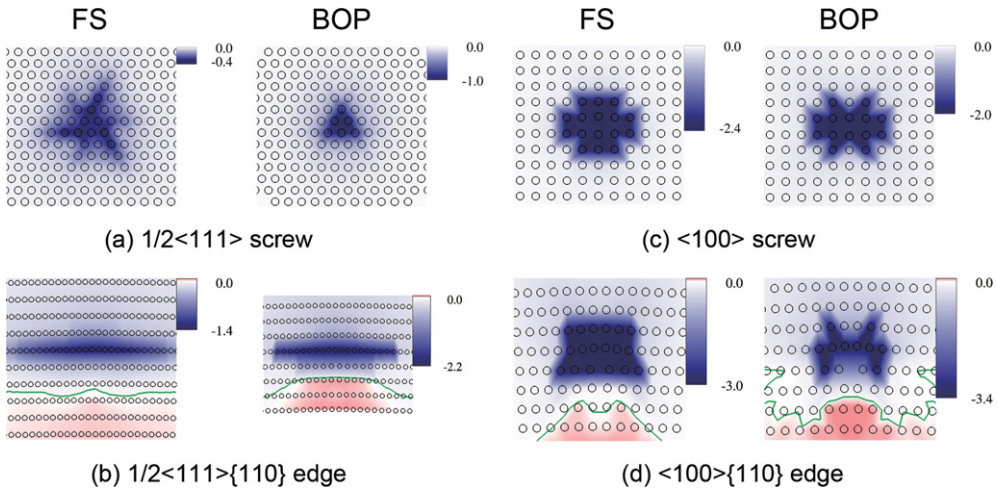

Figure 3. Binding energy maps showing the binding energy for the vacancy around the dislocations from figure 2. For edge dislocations, the green lines are the contour line corresponding to zero binding energy.

both the dislocation and the vacancy, respectively. According to this definition, the vacancy is attracted to the dislocation when E_{bind} is negative.

The vacancy formation energies calculated using BOP and FS potentials are presented in table 2. For the FS potential the vacancy formation energy is in fact a fitted quantity and thus it agrees closely with the results of both first-principles calculations and experimental data. The prediction of the BOP model is also good even though the vacancy formation energy is not included in the fitting database. Nevertheless, the absolute value of the vacancy formation energy is likely to have only a marginal influence on the dislocation–vacancy binding energy since E_{bind} is a relative quantity resulting from a subtle interplay of more contributions.

The computed vacancy binding energies as a function of the vacancy position are displayed in figure 3. From the binding energy maps we can conclude several things. First, the binding energies for the screw dislocations are always negative, indicating that they would act as sinks for the vacancies. The most favorable position for the vacancy is located in the core region of the screw, where the atoms are most distorted from their equilibrium positions. The binding of the vacancy to the core can also be interpreted as a creation of a double jog with a width of one lattice spacing along the $\langle 1\,1\,1\rangle$ direction [51–53].

Second, for the edge dislocations the obtained binding energies can be both positive and negative depending on the vacancy position. The negative energies corresponding to vacancy attraction occur predominantly in the region of compressive stress above the dislocation center. This observation agrees with previous studies of dislocation–vacancy interactions in other bcc metals using simple pair potentials [11, 12]. However, our calculations also show that the

binding energies on several atomic layers below the glide plane are slightly positive. This repulsion between the edge dislocations and the vacancy was not reported in the older studies, but it was found in more recent simulations employing the FS potentials [14, 15].

Third, the magnitudes of the binding energies vary significantly among the investigated dislocations. We obtained the smallest absolute values for the $1/2\langle 1\,1\,1\rangle$ screw. This result is not unexpected since the local atomic densities within the core are almost the same as in the bulk and only the bond angles are distorted. In contrast, the cores of the remaining three dislocations present much stronger disturbances to the crystal lattice in terms of both atomic densities and bond angles, which are reflected by larger binding energies exceeding 1 eV.

Finally, some differences exist between results calculated using BOP and FS potentials. For most dislocations studied here, BOP yields more compact core structures than the FS potential. Since the smaller cores are likely to be associated with larger local compressive stresses, it is understandable that BOP also yields larger binding energies due to larger release of the elastic energy when the vacancy is absorbed. However, the overall extent and shape of the most binding regions are generally similar with BOP and FS potentials, and follow closely the shape and the symmetry of the dislocation cores.

4. Comparison of atomistic results with elasticity theory

According to the elasticity theory, the interaction between a dislocation and a vacancy can be written as a sum of the first- and second-order size interactions and the inhomogeneity interaction [7, 8, 14, 42, 54]. The first-order size interaction arises from the interaction between the long-range stress field of the dislocation and the hydrostatic tension caused by lattice contraction around the vacancy [55]. Its form is usually deduced using a continuum model, where the crystalline body is replaced by an elastic medium with the dislocation simulated by an appropriate Volterra dislocation and the point defect by an elastic inclusion. The associated elastic energy can then be written as

$$E_1 = -\delta \int_V p_{ii}\,\mathrm{d}V, \tag{2}$$

where the integral is over the volume V, δ is the vacancy dilatation and p_{ii} is the hydrostatic stress due to the presence of the dislocation. If we assume tungsten as an isotropic medium, there will be no first-order size interaction between the vacancy and the screw dislocation since p_{ii} is zero. If the dislocation is of edge type, E_1 has an explicit form:

$$E_1 = \frac{4(1+\nu)\mu b\delta r_0^3 \sin\theta}{3(1-\nu)}\frac{1}{r}, \tag{3}$$

where μ, ν, b, r_0, r and θ are the shear modulus, Poisson's ratio, Burgers vector, radius of the unrelaxed vacancy, separation distance between the vacancy and the dislocation center, and vacancy–dislocation relative angle, respectively (see figure 1). The vacancy dilatation δ is expressed as

$$\delta = \frac{3\varepsilon(1-\nu)}{(1+\nu)}, \tag{4}$$

where ε corresponds to the change in vacancy radius due to relaxation, i.e. $\varepsilon = r_{\mathrm{rel}}/r_0 - 1$ where r_{rel} is the radius of the relaxed vacancy. The change in the vacancy radius can be either obtained directly from atomistic simulations or estimated within the harmonic approximation [12] as

$$\varepsilon = \sqrt[3]{\frac{3(c_{44}-c_{12})}{c_{11}+2c_{12}}+1} - 1. \tag{5}$$

Table 3. Elastic constants of tungsten (GPa).

C_{11}	C_{12}	C_{44}	μ	ν
522.4	204.4	160.6	160.0	0.28

Thus, all parameters required to compute the first-order contribution can be given within the framework of the elasticity theory.

The second-order size interaction originates from the non-linear elastic properties of the crystal [56] and its analytical derivation is too complicated to handle. Fortunately, since the vacancy relaxation is very small in metals such as W and Fe, the second-order contribution is small and can be neglected [7].

The inhomogeneity interaction arises from the differences in elastic constants (e.g. μ, B) between the matrix and the inclusion (vacancy in our case) [57]. As the elastic constants associated with the vacancy have to be lower than those of the matrix, the inhomogeneity interaction is always attractive. The presence of a vacancy then leads to a release of the elastic energy:

$$E_3 = \tfrac{1}{2} V p_{ij} e^{\mathrm{I}}_{ij}, \tag{6}$$

where e^{I}_{ij} is an induced strain, which is linearly related to the dislocation strain field [8, 57]. For a straight screw dislocation equation (5) is equal to

$$E_3 = \frac{5\mu b^2 r_0^3 (1-\nu)}{2\pi(7-5\nu)} \frac{1}{r^2}, \tag{7}$$

while for edge dislocations an additional dependence on angle appears as

$$E_3 = \frac{5\mu b^2 r_0^3}{2\pi(1-\nu)(7-5\nu)} \left[1 - \frac{1+6\nu-5\nu^2}{5} \sin^2\theta\right] \frac{1}{r^2}. \tag{8}$$

The presented theoretical predictions assume perfect dislocations and isotropic elasticity. In the case of W, the anisotropy ratio A is about 1.01, so that the use of isotropic elasticity is valid [42]. For the elastic calculations, we used the shear modulus μ and the Poisson coefficient ν (see table 3), obtained by the Voigt average of the elastic constants corresponding to the potential used for the atomistic calculations [42].

In figure 4, detailed comparisons between the elasticity theory predictions and the atomistic results of both FS potential and BOP are presented for different separation distances between the dislocations and the vacancies. The inset bar charts show the differences between the atomic results and the elasticity predictions. Since the interactions between the vacancy and edge dislocations depend on the relative angle θ between them (see equations (3) and (8)), we plot here as an example only one specific direction for both edge dislocations. A complete set of results is then shown in figure 5.

As illustrated in figure 4, the interaction energies calculated using the elasticity theory and those from the atomistic simulations agree well with each other provided that the separation distance between the dislocation core and the vacancy is larger than about 0.5 nm. As expected, (see the bar chart insets), large deviations from the elasticity predictions occur when the vacancy enters the dislocation core. The absorption of the vacancy leads to a local reconstruction of the core that can no longer be captured by continuum models. The large values of the binding energies within the cores indicate that all dislocations can be regarded as effective sinks for vacancies.

For edge dislocations, the magnitude of the interaction depends not only on the separation distance but also on the angle θ between the dislocation glide plane and the vector pointing

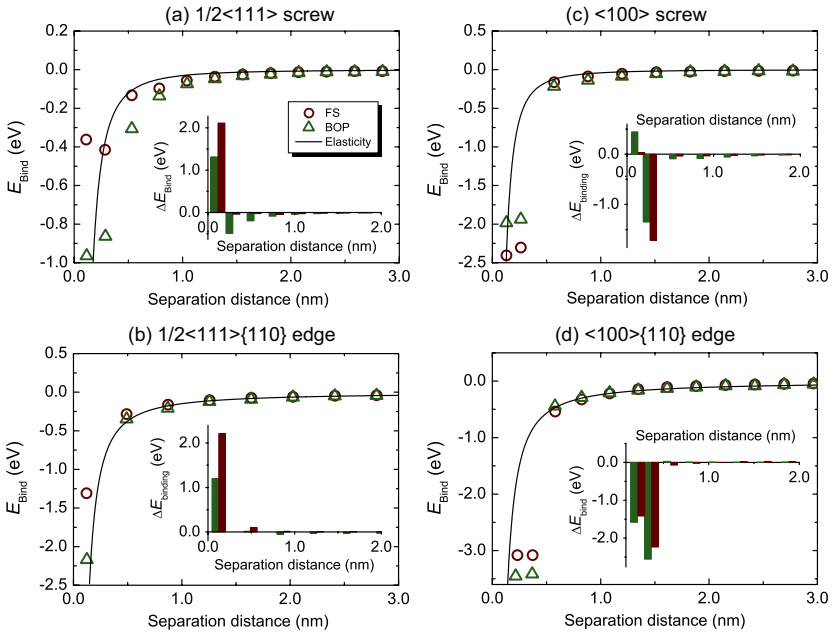

Figure 4. Dependences of the binding energies on the separation distance between the vacancy and the dislocation center. The plots show comparisons between the elasticity predictions (lines) and the atomistic results (points) for the dislocations from figure 2; the inset bar charts display the differences between the elasticity and atomistic results. Since for edge dislocations the interaction depends on the relative angle, only specific directions, namely $\langle 2\,0\,1\rangle$ for the $1/2\langle 1\,1\,1\rangle\{1\,1\,0\}$ edge dislocation and $\langle 1\,1\,1\rangle$ for the $\langle 1\,0\,0\rangle\{1\,1\,0\}$ edge dislocation, are plotted here.

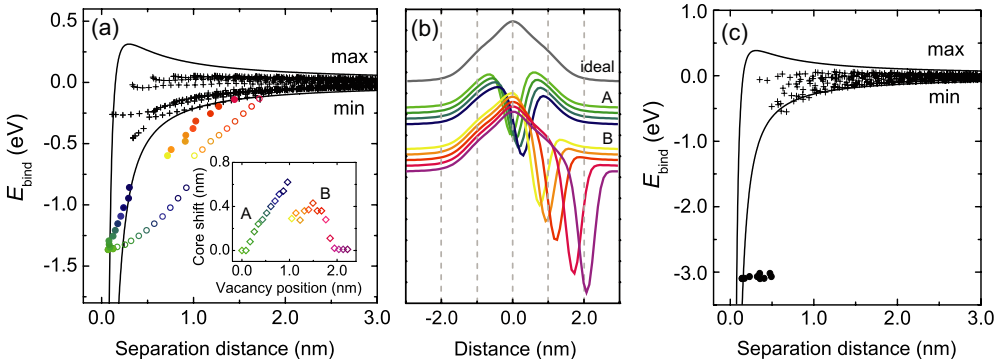

Figure 5. Dependences of the binding energies on the separation distance for edge dislocations. (*a*) and (*c*) show comparisons between the elastic range and the complete set of atomistic results for the $1/2\langle 1\,1\,1\rangle\{1\,1\,0\}$ and the $\langle 1\,0\,0\rangle\{1\,1\,0\}$ edge dislocations, respectively. The circles mark the most attractive sites for the vacancy located in the compressive region of the dislocation cores. The empty and full circles in (*a*) correspond to the vacancy positions before and after the relaxation, respectively. The magnitude of the corresponding vacancy-induced shifts of the $1/2\langle 1\,1\,1\rangle\{1\,1\,0\}$ core is shown as a function of the initial vacancy position in the inset plot. The separation distance after the relaxation was determined by analyzing the Burgers vector distributions displayed in (*b*). See text for detailed discussion.

from the dislocation center to the vacancy. Given a fixed separation distance, the minimum and the maximum of the interaction energy can be computed using equations (3) and (8). In figure 5 both the minimum and the maximum curves of the elasticity prediction are plotted, together with the atomistic results for all possible vacancy positions around the two edge dislocations calculated using the FS potential. The comparisons show that almost all results from the atomistic calculations fall in between the minimum and maximum boundaries given by the elasticity. The points lying outside this region are again for configurations in which the vacancy enters the dislocation core. For the $1/2\langle 1\,1\,1\rangle$ edge dislocation, these points correspond to vacancy positions located in the most attractive area on the plane immediately above the glide plane (see figure 3). We observed in our simulations that for these configurations the attractive interaction between the vacancy and the dislocation is so large that it causes the dislocation to move towards the vacancy. Figure 5(*a*) therefore shows two sets of symbols—empty circles corresponding to the initial separation distance, and full circles showing an estimated distance between the defects after relaxation. The magnitudes of the vacancy-induced dislocation shifts are shown in the inset of figure 5(*a*). The shifts were determined by analyzing and comparing the Burgers vector distributions of the vacancy containing cores along the $\{1\,1\,0\}$ glide plane. As mentioned above, the Burgers vector of the $1/2\langle 1\,1\,1\rangle\{1\,1\,0\}$ edge dislocation is rather widely spread along the slip plane, and the dislocation position can be determined from the continuous distribution of infinitesimal dislocation Burgers vector [50, 58, 59]. Figure 5(*b*) shows the Burgers vector distributions for an ideal dislocation core (top) and for relaxed cores containing vacancies, whose positions correspond to the minimum peaks on the curves. In both figures 5(*a*) and (*b*) we can clearly distinguish between two groups of configurations, marked as A and B. If the initial position of the vacancy is less than 1 nm from the core center and on the plane right above the glide plane (group A), the strong attraction pulls the dislocation closer to the vacancy with the shift being roughly linearly proportional to the initial separation (see the inset of figure 5(*a*)). As seen in figure 5(*b*), for all configurations in group A the vacancy is embedded in the very central region of the dislocation core, relieving its compressive stress. Interestingly, when the binding energies are plotted against the corrected separation distances (full points in figure 5(*a*)), the results fall again within the elastic limits. If the initial position of the vacancy is on the plane right above the glide plane but more than 1 nm from the core center (group B), the dislocation is still attracted by the vacancy but the effect is weaker and the dislocation shifts only by about 0.4 nm. The vacancy remains, in this case, in the border region of the core and even the corrected binding energies still lie outside the elastic range. Finally, when the initial separation is larger than about 2 nm, the dislocation position does not change during relaxation. It is interesting to note that the vacancy-induced dislocation shifts were observed by Ingle and Crocker [11] but not in other studies [12, 13, 36]. This may be related to the use of periodic simulation blocks containing stable dipole and quadrupole arrangements of dislocations in the latter studies rather than non-periodic blocks used here or by Ingle and Crocker. Additional studies of vacancy migration paths and barriers, which should provide more information about the dynamical aspects of the interactions, are currently in progress.

5. Discussion and conclusions

The present results provide detailed information about the vacancy–dislocation interaction energies in bcc tungsten and confirm that the vacancies are mostly attracted by the dislocations. The strength of the interaction, however, depends sensitively on the type of the dislocation as well as on the vacancy location. Based on large magnitudes of computed binding energies, the $\langle 1\,0\,0\rangle$ dislocation cores can be regarded as very strong sinks for vacancies. The vacancy

formation energies in these cores decrease to only a few tens of eV and are therefore dramatically reduced compared with a situation when the vacancy is located in the bulk crystal. It can be assumed that once trapped, the vacancy will stay attached to the $\langle 1\,0\,0\rangle$ core. The vacancy is also bound strongly to the most compressive region just above the slip plane of the $1/2\langle 1\,1\,1\rangle$ edge core. The attraction is so strong that it forces the dislocation to move towards the vacancy if the mutual separation is smaller than about 2 nm. This vacancy-induced dislocation glide is understandable, since the Peierls stress for the $1/2\langle 1\,1\,1\rangle$ edge dislocation is very low while the vacancy migration energy in W is about 2 eV [60]. The smallest binding for the vacancy is found in the $1/2\langle 1\,1\,1\rangle$ screw core. The likely reason is that this core is most bulk-like from all investigated cases and the changes in atomic bonding are mainly associated with variations of bond angles but not bond lengths, resulting in negligible changes of local hydrostatic stresses.

While it is clear from the thermodynamic point of view that the vacancy favors to be located in the vicinity of dislocation cores, the influence of segregated vacancies on dislocation mobility is much more complicated and can lead to different outcomes. First, the vacancy can act as a pinning site and hence hinder the dislocation glide. This scenario is most likely to occur at low temperatures and in the case of highly mobile edge and mixed dislocations that have extended planar cores and low Peierls stresses. The strong binding makes the vacancy–dislocation complex stable and sessile since its glide is governed by the thermally activated migration of the vacancy rather than applied stress. The situation can be, however, opposite for the $1/2\langle 1\,1\,1\rangle$ screw dislocation. The mobility of this dislocation at low temperatures is determined by a thermally activated formation of pair of kinks that can be enhanced if a vacancy is segregated at the dislocation core. Indeed, our preliminary calculations show that the Peierls barrier is significantly reduced when the vacancy is located in front of the screw dislocation. Finally, at high temperatures the non-conservative motion of dislocations occurs via diffusion of vacancies to/from dislocation cores [15, 52, 53], a process that depends both on the vacancy–dislocation binding and on the vacancy diffusion barriers and their variation in the vicinity of dislocation cores. Since the processes mentioned above depend sensitively not only on the binding of the vacancy to the dislocation core, they cannot be thoroughly analyzed based on the results presented here. Additional calculations of vacancy migration paths and barriers that would enable theoretical estimation of the vacancy diffusion to, from and along dislocations, and that would help to quantify the effects of vacancies on dislocation mobilities are currently in progress.

To summarize, the interaction between a vacancy and several dislocations in bcc tungsten was studied by means of the elasticity theory as well as atomistic calculations using two interatomic potentials. Four types of dislocations with the shortest Burgers vectors in the bcc lattice were included in our investigation. The results show that the dislocation–vacancy interactions can be well described by the linear elasticity as a free vacancy subjected to the elastic field of a dislocation when the separation distance between the two defects is larger than about 0.5 nm. For screw dislocations, it is accurate enough to predict the mutual elastic interaction by means of the inhomogeneity effect only. However, this effect has a much smaller contribution in the case of edge dislocations, for which the first-order size interaction dominates. When the separation distance between the dislocation center and the vacancy is less than 2–3 Burgers vectors the elasticity theory is no longer applicable and an explicit atomistic treatment is necessary.

Our simulations show rather good agreement between the results from BOP and FS potentials. Both potentials agree well with elasticity predictions when the separation distance exceeds the radius of dislocation core. For the $\langle 1\,0\,0\rangle$ dislocation cores, even the absolute values of the binding energies obtained from the two potentials agree well. The largest

differences are found for the $1/2\langle 1\,1\,1\rangle$ cores. BOP predicts the cores to be more compact and, consequently, the binding energies are about twice as large as those given by the FS potential. In the case of the $1/2\langle 1\,1\,1\rangle$ screw, the binding energy map of FS (cf figure 4) follows the shape of the degenerate core that is extended on three $\{1\,1\,0\}$ planes, while BOP yields correctly the non-degenerate core structure with the most favorable vacancy positions located at the core center. Since BOP is able to capture non-central bonding effects associated with changes of not only bond lengths but also of bond angles [61, 62], BOP results are likely to be more accurate than those obtained using the FS potential, especially for the $1/2\langle 1\,1\,1\rangle$ dislocations.

Acknowledgments

The authors wish to acknowledge the support by the German Science Foundation, grant MR 22/5-1, and by the German Federal Ministry of Education and Research BMBF, grant 03X0511.

AQ2

References

[1] Legros M, Dehm G, Arzt E and Balk T J 2008 Observation of giant diffusivity along dislocation cores *Science* **319** 1646–9
[2] Cuitino A M and Ortiz M 1996 Ductile fracture by vacancy condensation in fcc single crystals *Acta Mater.* **44** 427–36
[3] Bacon D J, Osetsky Y N and Rodney D 2009 *Dislocations in Solids* ed J P Hirth and L Kubin (Amsterdam: Elsevier)
[4] Eldrup M and Singh B N 2003 Accumulation of point defects and their complexes in irradiated metals as studied by the use of positron annihilation spectroscopy—a brief review *J. Nucl. Mater.* **323** 346–53
[5] Gumbsch P 2003 Brittle fracture and the brittle-to-ductile transition of tungsten *J. Nucl. Mater.* **323** 304–12
[6] Gumbsch P, Riedle J, Hartmaier A and Fischmeister H F 1998 Controlling factors for the brittle-to-ductile transition in tungsten single crystals *Science* **282** 1293–5
[7] Bullough R and Newman R C 1963 The interaction of vacancies with dislocations *Phil. Mag.* **7** 529
[8] Bullough R and Newman R C 1970 The kinetics of migration of point defects to dislocations *Rep. Prog. Phys.* **33** 101–48
AQ3
[9] Hirsch P B 1960 *Proc. 5th Int. Conf. on Crystallography* (Cambridge: Cambridge University Press) p 139
[10] Li J, Ngan A H W and Gumbsch P 2003 Atomistic modeling of mechanical behavior *Acta Mater.* **51** 5711–42
[11] Ingle K W and Crocker A G 1978 Interaction between vacancies and 1/2[1 1 1](1 1 0) edge dislocation in body-centered cubic metals *Acta Metall.* **26** 1461–9
[12] Miller K M 1981 Point defect–dislocation interactions in molybdenum *J. Phys. F: Met. Phys.* **11** 1175–89
[13] Masuda K 1980 On the interaction between a vacancy and a dislocation in metals *Phys. Status Solidi* b **99** 593–8
[14] Clouet E 2006 The vacancy–edge dislocation interaction in fcc metals: a comparison between atomic simulations and elasticity theory *Acta Mater.* **54** 3543–52
[15] Lau T T, Lin X, Yip S and Van Vliet K J 2009 Atomistic examination of the unit processes and vacancy–dislocation interaction in dislocation climb *Scr. Mater.* **60** 399–402
[16] Kabir M, Lau T T, Rodney D, Yip S and Van Vliet K J 2010 Predicting dislocation climb and creep from explicit atomistic details *Phys. Rev. Lett.* **105** 095501
[17] Woodward C and Rao S I 2001 *Ab-initio* simulation of isolated screw dislocations in bcc Mo and Ta *Phil. Mag.* A **81** 1305–16
[18] Cottrell A H and Pettifor D G 1992 *Electron Theory in Alloy Design* (London: Institute of Materials, Minerals and Mining)
[19] Yip S 2005 *Handbook of Materials Modeling* (New York: Spinger)
[20] Finnis M W and Sinclair J E 1984 A simple empirical *n*-body potential for transition-metals *Phil. Mag.* A **50** 45–55
[21] Kohlhoff S, Gumbsch P and Fischmeister H F 1991 Crack propagation in bcc crystals studied with a combined finite-element and atomistic model *Phil. Mag.* A **64** 851–78
[22] Cheng Y, Mrovec M and Gumbsch P 2008 Atomistic simulations of interactions between the $1/2\langle 1\,1\,1\rangle$ edge dislocation and symmetric tilt grain boundaries in tungsten *Phil. Mag.* **88** 547–60

[23] Cheng Y, Mrovec M and Gumbsch P 2008 Crack nucleation at the Σ9(2 2 1) symmetrical tilt grain boundary in tungsten *Mater. Sci. Eng.* A **483–484** 329–32
[24] Pettifor D G 1995 *Bonding and Structure of Molecules and Solids* (Oxford: Oxford University Press)
[25] Pettifor D G, Aoki M, Gumbsch P, Horsfield A P and Manh D N 1995 Defect modelling: the need for angularly-dependent potentials *Mater. Sci. Eng.* A **192/193** 24–30
[26] Horsfield A P, Bratkovsky A M, Fearn M, Pettifor D G and Aoki M 1996 Bond-order potentials: theory and implementation *Phys. Rev.* B **53** 12694
[27] Mrovec M, Groger R, Bailey A G, Nguyen-Manh D, Elsasser C and Vitek V 2007 Bond-order potential for simulations of extended defects in tungsten *Phys. Rev.* B **75** 16
[28] Mrovec M, Nguyen-Manh D, Pettifor D G and Vitek V 2004 Bond-order potential for molybdenum: application to dislocation behavior *Phys. Rev.* B **69** 094115
[29] Duesbery M S 1989 *Dislocations in Solids* (Amsterdam: North-Holland)
[30] Christian J 1983 Some surprising features of the plastic deformation of body-centered cubic metals and alloys *Metall. Mater. Trans.* A **14** 1237–56
[31] Duesbery M S and Vitek V 1998 Plastic anisotropy in bcc transition metals *Acta Mater.* **46** 1481–92
[32] Ohr S M and Beshers D N 1963 Crystallography of dislocation networks in annealed iron *Phil. Mag.* **8** 1343–60
[33] Benson R, Thomas G and Washburn J 1962 *Direct Observation of Lattice Defects in Crystals* (New York: Interscience Publishers)
[34] Louchet F and Kubin L P 1979 Dislocation processes in bcc metals *Phys. Status Solidi* a **56** 169–76
[35] Foxall R A, Duesbery M S and Hirsch P B 1967 Deformation of niobium single crystals *Can. J. Phys.* **45** 607
[36] Bullough R and Perrin R C 1968 *Dislocation Dynamics* (New York: McGraw-Hill)
[37] Gehlen P C, Rosenfield A R and Hahn G T 1968 Structure of the ⟨1 0 0⟩ edge dislocation in iron *J. Appl. Phys.* **39** 5246–54
[38] Sinclair J E 1971 Improved atomistic model of a bcc dislocation core *J. Appl. Phys.* **42** 5321–9
[39] Gehlen P C, Hoagland R G, Hirth J P and Kanninen M F 1972 New representation of strain field associated with cube-edge dislocation in a model of a alpha-iron *J. Appl. Phys.* **43** 3921
[40] Ackland G J and Thetford R 1987 An improved *n*-body semiempirical model for body-centered cubic transition-metals *Phil. Mag.* A **56** 15–30
[41] Osetsky Y U and Bacon D J 2003 An atomic-level model for studying the dynamics of edge dislocations in metals *Modelling Simul. Mater. Sci. Eng.* **11** 427–46
[42] Hirth J P and Lothe J 1982 *Theory of Dislocations* (New York: Wiley)
[43] Bitzek E, Koskinen P, Gahler F, Moseler M and Gumbsch P 2006 Structural relaxation made simple *Phys. Rev. Lett.* **97** 4
[44] Sigle W 1999 High-resolution electron microscopy and molecular dynamics study of the (a/2)[1 1 1] screw dislocation in molybdenum *Phil. Mag.* **79** 1009–20
[45] Mendis B G, Mishin Y, Hartley C S and Hemker K J 2006 Use of the Nye tensor in analyzing HREM images of bcc screw dislocations *Phil. Mag.* **86** 4607–40
[46] Moriarty J, Vitek V, Bulatov V and Yip S 2002 Atomistic simulations of dislocations and defects *J. Comput. Aided Mater. Des.* **9** 99–132
[47] Vitek V 2004 Core structure of screw dislocations in body-centred cubic metals: relation to symmetry and interatomic bonding *Phil. Mag.* **84** 415–28
[48] Vitek V 1974 *Cryst. Latt. Defects* **5** 1
[49] Groger R and Vitek V 2009 Directional versus central-force bonding in studies of the structure and glide of 1/2 <1 1 1> screw dislocations in bcc transition metals *Phil. Mag.* **89** 3163–78
[50] Yamaguchi M and Vitek V 1972 Core structure of nonscrew 1/2⟨1 1 1⟩ dislocations on {1 1 0} planes in bcc crystals: I. Core structure in an unstressed crystal *J. Phys. F: Met. Phys.* **3** 523–36
[51] Thomson R M and Balluffi R W 1962 Kinetic theory of dislocation climb: I. General models for edge and screw dislocations *J. Appl. Phys.* **33** 803
[52] Balluffi R W 1970 On measurements of self-diffusion rates along dislocations in fcc metals *Phys. Status Solidi* **42** 11
[53] Balluffi R W and Thomson R M 1962 Kinetic theory of dislocation climb: II. Steady state edge dislocation climb *J. Appl. Phys.* **33** 817
[54] Friedel J 1964 *Dislocations* (Oxford: Pergamon)
[55] Cottrell A H and Bilby B A 1949 Distribution of solute atoms around a slow dislocation *Proc. Phys. Soc. Lond. Ser.* A **62** 49
[56] Pfeiderer H, Seeger A and Kroener E 1960 *Z. Naturf.* a **15** 758
[57] Eshelby J D 1957 *Proc. R. Soc. Lond.* A **241** 376

[58] Vitek V, Lejcek L and Bowen D K 1971 *Interatomic Potentials and Simulation of Lattice Defects* ed P C Gehlen *et al* (New York: Plenum) pp 493–508
[59] Yamaguchi M and Vitek V 1974 Core structures of non screw 1/2⟨1 1 1⟩ dislocations on {1 1 2} planes of bcc crystals: I. Core structure in an unstressed crystal *J. Phys. F: Met. Phys.* **5** 1–10
[60] Willaime F, Satta A, Nastar M and Le Bacq O 2000 Electronic structure calculations of vacancy parameters in transition metals: impact on the bcc self-diffusion anomaly *Int. J. Quantum Chem.* **77** 927–39
[61] Mrovec M, Elsaesser C and Gumbsch P 2009 Interactions between lattice dislocations and twin boundaries in tungsten: a comparative atomistic simulation study *Phil. Mag.* **89** 3179–94
[62] Mrovec M, Elsaesser C and Gumbsch P 2010 Atomistic simulations of lattice defects in tungsten *Int. J. Ref. Met. Hard Mater.* **28** 698–702

QUERIES

Page 1
AQ1
Please be aware that the colour figures in this article will only appear in colour in the web version. If you require colour in the printed journal and have not previously arranged it, please contact the Production Editor now.

Page 12
AQ2
Please check the details for any journal references that do not have a blue link as they may contain some incorrect information. Pale purple links are used for references to arXiv e-prints.

Page 12
AQ3
Please provide place of Conference for reference [9].